2022 IEEE/ASME International Conference on
Advanced Intelligent Mechatronics (AIM)

2022 IEEE/ASME International Conference on Advanced Intelligent Mechatronics (AIM) | 978-1-6654-1308-4/22/$31.00 ©2022 IEEE | DOI: 10.1109/AIM52237.2022.9863300

Adaptive Deposit Compensation of Construction Materials in a 3D Printing Process

Xinrui Yang, Othman Lakhal, Abdelkader Belarouci and Rochdi Merzouki

Abstract— Additive Manufacturing (AM), known as 3D Printing (3DP), has been widely implemented in the industry due to its advantage of free design and high efficiency in rapid prototyping. Recently, 3D Construction Printing (3DCP) has become an emerging topic. As a multidisciplinary subject, it involves a complex system that consists of multiple subsystems, the uncertainty of material behaviour also bring risks to the printing quality. Hence, the main issue of 3DCP lies in the online monitoring and control of the printing process quality. This paper presents a combined approach for online 3D construction material printing quality monitoring and adaptive compensation for printing layer. The width of freshly printed filament can be adopted to characterize the printing quality. A vision system based on Deep Learning is developed to detect automatically the filament width deviation. Based on the results of the vision system, a real time adaptive compensation of the nozzle travel speed is realized to maintain the quality deposit performance. The proposed approach is validated by on site printing experiments.

I. Introduction

Additive manufacturing (AM), also known as 3D Printing (3DP), has been widely applied in the field of industry manufacturing. In recent years, the application of 3D Construction Printing (3DCP) is emerging in the field of civil engineering, thanks to its advantages including significant labor reduction [1], high design freedom, high efficiency in term of construction time and material usage [2], [3]. Its ability to use recycled material generated from construction wastes also proves its value in environmentally friendly construction [4].

Investigation shows that there exists two categories of printing methods: injection method and extrusion/deposition method [5]. The latter is the most commonly used. In [6], the authors design and study the control of a Mobile Manipulator Robot for 3DCP using clay or concrete materials, the accurate guidance of printing nozzle is achieved.

In the context of this paper, we consider robotized 3DCP system using deposition based method. The process of robotized 3DCP contains multiple steps. Firstly, the shape of the structure to be printed is designed by 3D Computer-Aided Design technology. Secondly, with the help of slicer software, a trajectory of material deposition is generated. Thirdly, the robot in the printing system executes the trajectory given by the slicing step, guiding the nozzle to realize material deposition of Fig. 1.

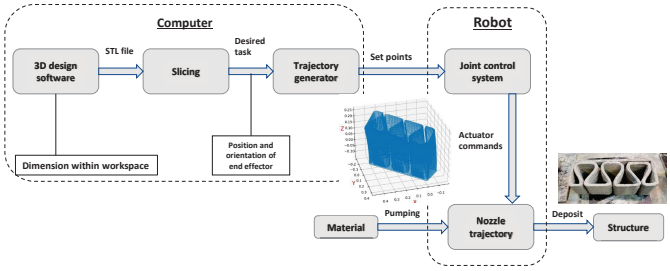

Fig. 1: Procedure of 3D Construction Printing

The quality control of printing process is one of the main subjects in 3DCP. As a multidisciplinary topic concerning robotics, material and control theory, the closed-loop control of 3D printing systems is one of the main issues.

Studies have been conducted on the modeling and control of ink-jet 3D printing system [7], [8], in order to maintain the shape consistency of printed product.

Due to the multidisciplinary process of 3DCP, the causes of abnormal behavior during printing process can come from different part of the system. On the one hand, during the printing process, the material is in transient stage, under the pump pressure and due to environmental features, its internal chemical reaction will impact the material behavior, especially when the printing process is performed outdoors [9]. Some criteria are adopted as key factors to evaluate the material deposition quality, such as printing filament surface finishing and deformation [10]–[12]. As the filament deformation can be easily quantified, it is widely used to evaluate printing quality. Investigations show that other than rheology properties of the material, printing filament deformation is also significantly affected by printing system parameters (e.g. nozzle travel speed) [13]–[15]. However, conventional 3DCP control method requires time-cost pre-calibration of printing system, which also highly depends on material properties and the stability of pumping system [16].

Thus, real time quality monitoring system is required in order to control the nozzle travel speed adaptively in order to compensate the filament deformation.

Various approaches have been developed to characterize the filament width or to compensate width deviation during the printing procedure. In [17], the authors employed a 3D structured light scanning system for evaluating

Xinrui Yang, Othman Lakhal, Abdelkader Belarouci and Rochdi Merzouki are with University of Lille, CRIStAL, CNRS-UMR 9189, Avenue Paul Langevin, 59655 Villeneuve d'Ascq, France. xinrui.yang@univ-lille.fr

the clay printing quality in the post-printing stage by measuring layer dimensions. 3D LiDAR are also used to detect printing layer deformation, but in post-printing stage [18]. Computer Vision (CV) methods (e.g. edge detection) based on 2D images have also been adopted for the identification of printing filament [19]. However, conventional CV methods usually require high contrast between the target and the background and can be highly affected by light condition, shadow, noise, as well as the finishing on filament surface.

Recently, with the bloom of Artificial Intelligence (AI) and significant increase in computer computing power, Deep Learning (DL) methods based on Convolutional Neural Networks (CNNs) have proved their ability in image feature extraction, they exceed traditional CV methods in robust performance and generalization ability. Those methods are implemented in various fields. In [20] a DL segmentation model has been implemented in post-printing stage to analyze layer height deformation for a large scale 3DCP product, but in this study the model is only used to extract the entire printed structure, the layer detection is done with conventional edge detection.

In this work, the filament width is adopted as the factor to characterize the printing quality. A Deep Learning instance segmentation model is adopted. A contact-free real time printing monitoring system based on the trained model is developed to track filament width deviation. The online adaptive compensation control for filament width deviation is then realized. This adaptive compensation method does not require high cost 3D scanning devices and is less influenced by background noises. Experimental results prove the feasibility and performance of this novel approach. The paper is organised as follows: Section II is dedicated on the DL-based automatic detection of the filament width, Section III concerns the adaptive printing filament width compensation, Section IV concerns the experimental tests, while Section V concludes on the proposed results.

II. Filament segmentation and width calculation

In this part, a vision system is developed to perform the detection of printing filament and to send alarm when filament width deviation occurs. The system consists of two cameras placed on the printing system and a computer that is in charge of communication with the robot. Printing filaments with different curvature and surface finishing quality can be detected under various light conditions. The methodology is based on Deep Learning CNNs, morphology and coordinate transformation. It can be divided into three steps: filament segmentation, center line extraction and width calculation.

A. Filament Segmentation

1) Dataset Preparation: We prepared an image dataset of 3DCP filament with the help of the two cameras fixed to the nozzle. The dataset contains 400 images of printing filament from top view. The images are collected during several printing tests in different light conditions, with different printing beds, different nozzle trajectory, different width and is being updated after each new printing test.

A pre-processing step is applied to the images in the dataset. Firstly, as the camera is fixed to the nozzle, the nozzle outlet position is fixed in the image, hence the image can be cropped according to the RoI (region of interest) that contains only the nozzle tip and new deposited filaments. This step helps to reduce the computational time of the system. Secondly, data augmentation methods are used to enhance the diversity of the dataset, including image flipping, artificial shadow and blur. This step enhance the model's resistance to environmental interference.The final step is data annotation, a polygon is created for each filament instance in order to segment the pixels belonging to the target (i.e. filament) from the image.

2) Instance Segmentation Model: An instance segmentation model is constructed and trained upon pytorch platform. The selected model is Mask RCNN due to its performance in high precision and inference speed. The training session is carried out with an NVIDIA Quadro RTX3000 GPU. After 800 iterations of training, the total loss function of the model converges. We built a validation dataset containing 150 images to evaluate the model performance in instance segmentation. The segmentation evaluation results of the model on the validation dataset gives 88.8% Average Precision at 0.5 IoU (AP50) and 79.8% Average Precision at 0.75 IoU (AP75).

Given a top view image of filament taken by the camera as input, the output of the model contains 3 parts: a confidence score of the result, a bounding box that contains the target area and a binary mask that classify each pixel into target or background. Fig.2 shows the output example of the model. The resolution of the cameras used in this work is $492x658$ pixels.

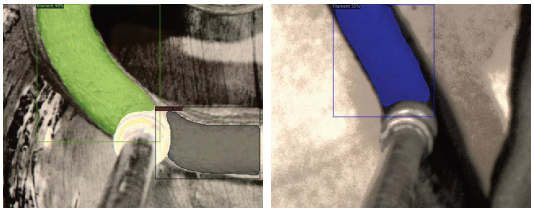

Fig. 2: Outputs of filament segmentation model

B. Center Line Extraction

In this step, the morphological medial axis transform method (also referred to as image skeletonization) is adopted to extract a center line of the detected filament. In the image coordinate system, given S the set of pixels of the filament region bounded by its contour C, the center line of the filament is the set of points $P \in S$ that have more than one closest point on the contour C. AS the segmentation model gives a binary mask representing the

filament, by applying medial axis transform on the binary mask, we can locate pixels on the filament center line, and compute the local width (pixel unit) of the filament at each pixel on the center line.

Fig.3 shows an example result of filament center line in the image frame. We can see that the filament contour has an overall rectangle-like appearance, however, at the two ends ($E1$, $E2$) in green circle, the local widths don't match the width of the filament. Thus, we consider only the local widths at the middle part of the center line. The distribution of local width values along the center line is calculated, as shown in Fig.4 , the mode of local width values can represent the average width value (pixel unit) of the filament.

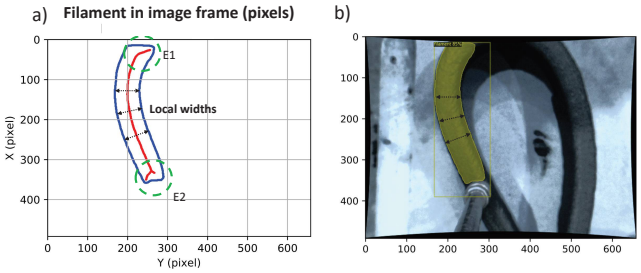

Fig. 3: Filament center line in image frame. a). local width values at two ends E1 and E2 can not represent the local width of filament. b). segmented filament from image captured by visual sensor.

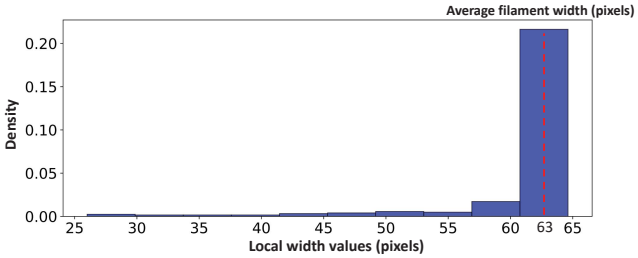

Fig. 4: Local width value distribution (pixel unit)

C. Automatic filament width calculation

When the average width of filament is obtained in the image frame, the width in real dimension can be calculated by applying frame transformation. As the camera is fixed to the nozzle, the distance d from the lens to the freshly printed filament is fixed. The optical axis of the camera is parallel to the nozzle, no rotation is considered. For a point $G = [a,b,0]^T$ in the image frame, its coordinate $P = [x,y,z]^T$ in the world frame is given by:

$$P(G) = R^{-1}(M^{-1}(s \cdot G) - t) \tag{1}$$

where:

- R the rotation matrix of camera with respect to world frame, which can be substituted with identity matrix.
- M the camera intrinsic matrix is obtained through camera calibration step.
- $t = [0,0,d]^T$ the translation vector of camera with respect to the world frame, where d is the distance from the camera to the new filament surface.

Hence, given the average width of the filament w_{pixel}, its real value in millimeter is equivalent to the distance from $P([0,0,0]^T)$ and $P([0,w_{pixel},0])^T$.

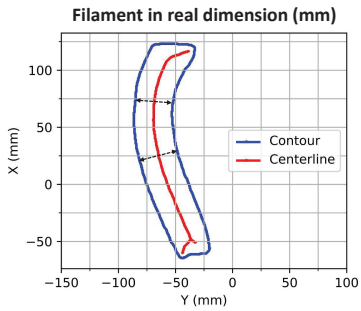

Fig. 5: Average filament width calculated in real dimension (35.5mm)

The processing time of the whole procedure from filament segmentation to width calculation upon one frame is around 0.2 s. As during the 3DCP process, the nozzle moves under low speed, the traveled distance between two frames is under 4cm. Furthermore, in real time application, we adopt a smaller region of interest so that the average width calculated by the algorithm can represent well the global width of the short freshly printed filament.

D. Undistortion calibration test

In order to obtain correct results when the detected target is close to the image edge, an undistortion step is applied to eliminate errors due to camera distortion. With the information, namely distortion coefficients obtained through camera calibration step, we can realize undistortion with the built-in function of OpenCV library. A $40mm \times 40mm$ ArUco marker is used to test the algorithm. As shown in Fig.6, the undistortion step significantly reduces the sum of squared errors (SSE) when calculating size of the four edges of the marker. Fig.7 shows an example of result of filament segmentation and width calculation tested on a filament specimen of printed piece. An error within 1mm is reached.

III. Adaptive printing filament width compensation

In this section, we develop the adaptive compensation for printing filaments based on the width calculation methodology described in section II. The objective is to realize an online adaptive compensation of the nozzle speed during the material deposition, based on the width estimation information of freshly printed filaments. The width is obtained from the DL-based automatic detection described in Section II, Fig.8 shows the real-time workflow of the DL-based automatic detection algorithm.

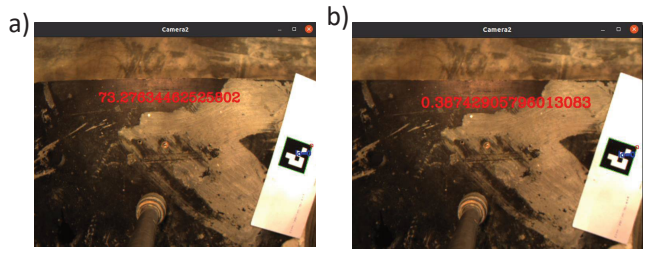

Fig. 6: a) without undistortion step, $SSE \approx 73.3mm^2$; b) with undistortion step, $SSE \approx 0.39mm^2$

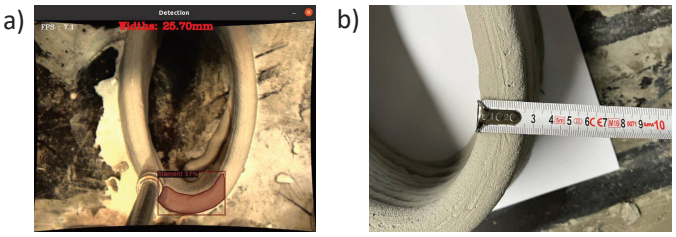

Fig. 7: Results of an automatic filament segmentation and width calculation. a). calculated width: 25.7mm b). measured width: 26mm.

During the printing procedure, the following relationship among the flow material rate $Q(mm^3/s)$, the filament width $w(mm)$, the filament height $h(mm)$, and nozzle travel speed $v(mm/s)$ can be established [21]:

$$Q = v.w.h \tag{2}$$

The material deposition rate $D(mm^2)$ [16] is defined as :

$$D = \frac{Q}{v} = w.h \tag{3}$$

We adopt the assumption that in the same filament, the real height h^m is identical to the desired filament height

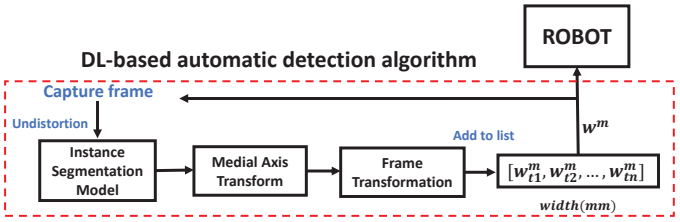

Fig. 8: Workflow of DL-based automatic detection algorithm

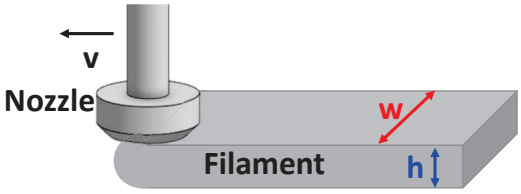

Fig. 9: Printing filament parameters

h^d. Fig.9 shows the model of the filament. The width deviation error during the printing process e_w is given as the difference between the desired filament w^d width and the measured one w^m from the DL-based automatic detection algorithm, as follows :

$$e_w = w^d - w^m \tag{4}$$

An admissible threshold to evaluate the width deviation error is decided, so that compensation should be performed when e_w exceeds the threshold $\pm\Delta$. This threshold is valuated at 10% of the nominal value of the width error, including all the uncertainties. Three cases of measured flow of material (Q^m) fluctuation is considered, according to the desired filament width ($w^d = 30mm$), the desired filament height (h^d) and the measured nozzle speed (v^m) as in Fig.10, during the printing process are studied:

- Case 1: if $Q^m = w^d h^d v^m$, $-\Delta < e_w < \Delta$, the filament matches desired width.
- Case 2: if $Q^m < w^d h^d v^m$, $e_w > \Delta$, the filament is too narrow.
- Case 3: if $Q^m > w^d h^d v^m$, $e_w < -\Delta$, the filament is too wide.

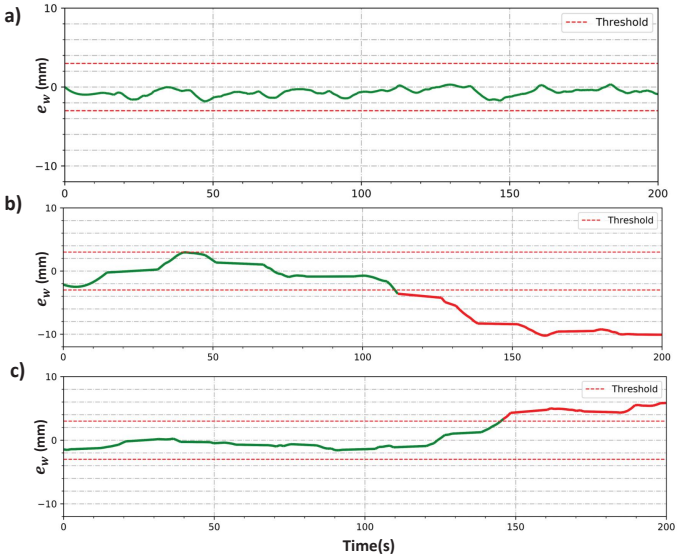

Fig. 10: The filament width error e_w during printing. Threshold is $\pm 3mm$ a) case 1: filament width is close to desired width; b) case 2: filament is too narrow; c) case 3: filament is too wide.

Let us consider that the dynamic of the nozzle guided by an industrial arm, operating in conditions of low speed and acceleration of Fig. 2. In the case of the nozzle system of a mass m with a viscous friction f, autonomously guided linearly with a speed of v^m in permanent printing mode, where its dynamic behaviour can be expressed as follows:

$$U = f.v^m + m.\dot{v^m} \tag{5}$$

Where U is the speed control of the nozzle of Fig. 11. To calculate this control law, the following development is

considered:

$$U = m.\dot{v^d} + f.v^d + K_p.\varepsilon + K_d.\dot{\varepsilon} + (\frac{Q^m}{D} - v^m).sign(e_w - \Delta) \quad (6)$$

Where K_p and K_d are the proportional and derivative parameters of the PD nozzle speed controller of Fig. 11, $\varepsilon = v^d - v^m$ is the nozzle speed error and the nonlinear *signum* function is added to switch between the compensation mode of nozzle speed (increase or decrease). After replacing (6) in (5), the following equation of the overall closed-loop system error is obtained between nozzle speed error and the width filament error:

$$(m + K_d).\dot{\varepsilon} + (f + K_p).\varepsilon = (v^m - \frac{Q^m}{D}).sign(e_w - \Delta) \quad (7)$$

This allows to adapt through an automatic compensation of the filament width using the nozzle speed when deviation occurs.

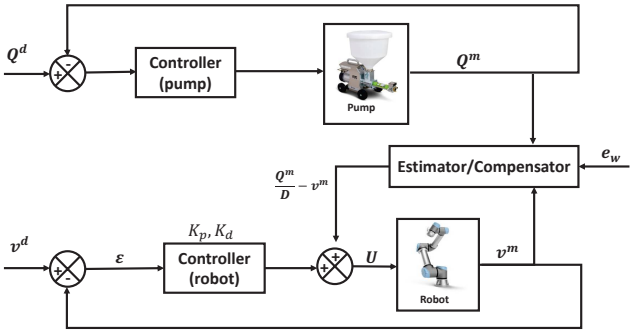

Fig. 11: Adaptive compensation control scheme

IV. Experimental Results in 3D printing site

A. 3D Printing System description

This work is realized on a robotized 3D printing system equipped with multiple sensors, using construction material including material recycled from construction wastes. The system, shown in Fig.12 consists of the following parts:

- A concrete mixer is used to prepare material according to the given batching.
- Pump: a MAI 2PUMP-PICTOR Mortar is used to generate the material flow going through a hose.
- Robot: a UR 10e collaborative manipulator robot with 6 DoF is used to execute the trajectory of printing. A nozzle of 30 mm diameter equipped with sensors is fixed to the end effector of the robot.
- Sensors: the system contains multiple sensors. A pressure sensor is installed at the inlet of the hose to monitor pump status. 2 Basler industrial Gigabit Ethernet (GigE) cameras are fixed on left and right side of the nozzle. The distance from camera lens to the nozzle outlet is 480mm.
- Computer: the control of robot and pump and the communication among different components of the system are realized via Robot Operation System (ROS) running on a computer.

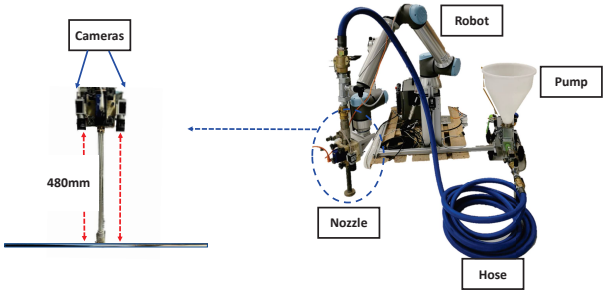

Fig. 12: Printing system

B. 3D Printing requirements and discussions

Printing experiments are carried out to validate the feasibility of the developed online adaptive layer compensation strategy. A 30 layer rectangle-shape structure is designed, with the theoretical layer width $w^d = 30mm$, height $h^d = 9mm$. The overall dimension of the shape is $80cm \times 10cm \times 27cm$ as shown in Fig.13.

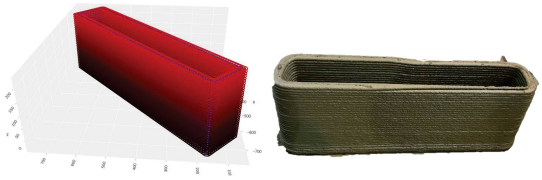

Fig. 13: The designed shape to print and the final printed shape.

We prepare the material according to the following concrete batching: 35 kg of cement, 38.5 kg of recycled sand, 12.1 kg of water, 875 g of superplasticizer and 70 g of viscosifier.

The printing experiment was conducted indoors with stable temperature (15°C) and humidity. The nozzle is guided by the UR 10e robot, the speed of robot Tool Center Point (TCP) is limited within 3 cm/s and 18 cm/s. During the printing, the pump voltage is varied in order to provoke fluctuation of pumping flow.

Fig.14 shows the measured filament width (mm), pump voltage (V) and nozzle travel speed (cm/s). We can see that due to fluctuation of pumping flow, width deviation occurs. When width error e_w exceeds the threshold and tend to stabilize, the controller compensate the filament width by regulating the nozzle travel speed. The filament width error returns to the tolerable range. The result demonstrates the adaptive compensation performed online during printing process.

V. CONCLUSIONS

This paper proposed an approach for the adaptive compensation of the filament width deviation for 3D printing using construction material. We adopted the width of freshly printed filament as the criterion to characterize printing quality. A DL-automatic detection algorithm is

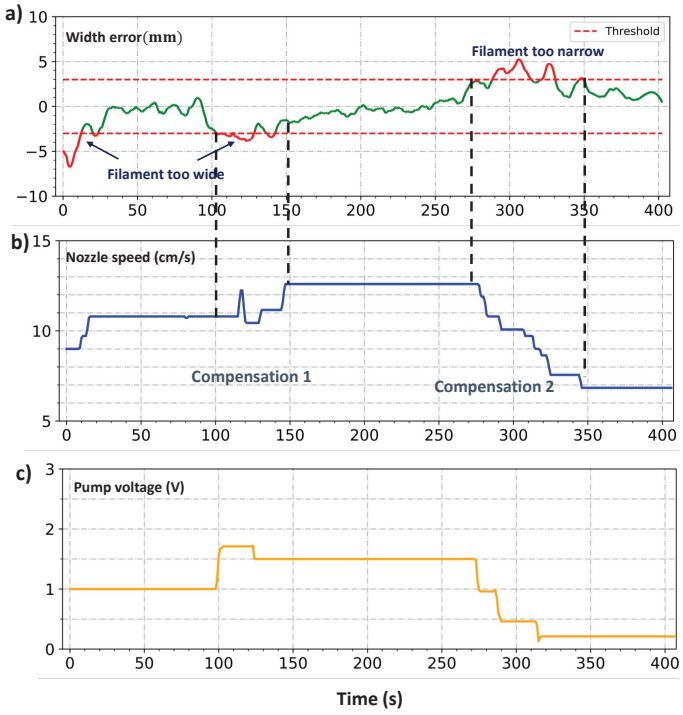

Fig. 14: Parameters during printing procedure. a).filament width error, red part exceeds threshold while green part stays in the tolerable range; b). Nozzle travel speed; c). pump voltage.

developed for the detection of printing filament and measure of its average width. The algorithm combines a DL instance segmentation model, the morphological medial axis transform and image frame transformation. The latter provide an input to a designed adaptive compensation control of the nozzle speed. Experiments prove the accurate performance of the joint automatic detection and adaptive compensation. These have shown that through nozzle travel speed regulation, the deviation of printing filament width can be controlled within the given threshold. For future work, the adaptive compensation with the height of the filament is to be considered.

ACKNOWLEDGMENT

This work has been realized with the support of EU funding through Interreg project CIRMAP NWE 1062.

References

[1] M. Hossain, A. Zhumabekova, S. C. Paul, J. R. Kim et al., "A review of 3d printing in construction and its impact on the labor market," Sustainability, vol. 12, no. 20, p. 8492, 2020.

[2] M. T. Souza, I. M. Ferreira, E. G. de Moraes, L. Senff, and A. P. N. de Oliveira, "3d printed concrete for large-scale buildings: An overview of rheology, printing parameters, chemical admixtures, reinforcements, and economic and environmental prospects," Journal of Building Engineering, vol. 32, p. 101833, 2020.

[3] P. Wu, J. Wang, and X. Wang, "A critical review of the use of 3-d printing in the construction industry," Automation in Construction, vol. 68, pp. 21–31, 2016.

[4] R. Mathur, "3d printing in architecture," International journal of innovative science, engineering & technology, vol. 3, no. 7, pp. 583–591, 2016.

[5] A. Perrot and S. Amziane, "3d printing in concrete: general considerations and technologies," 3D Printing of Concrete: State of the Art and Challenges of the Digital Construction Revolution, pp. 1–40, 2019.

[6] O. Lakhal, T. Chettibi, A. Belarouci, G. Dherbomez, and R. Merzouki, "Robotized additive manufacturing of funicular architectural geometries based on building materials," IEEE/ASME Transactions on Mechatronics, vol. 25, no. 5, pp. 2387–2397, 2020.

[7] L. Lu, J. Zheng, and S. Mishra, "A layer-to-layer model and feedback control of ink-jet 3-d printing," IEEE/ASME Transactions on Mechatronics, vol. 20, no. 3, pp. 1056–1068, 2014.

[8] U. Inyang-Udoh, Y. Guo, J. Peters, T. Oomen, and S. Mishra, "Layer-to-layer predictive control of inkjet 3-d printing," IEEE/ASME Transactions on Mechatronics, vol. 25, no. 4, pp. 1783–1793, 2020.

[9] J. Sun, J. Xiao, Z. Li, and X. Feng, "Experimental study on the thermal performance of a 3d printed concrete prototype building," Energy and Buildings, vol. 241, p. 110965, 2021.

[10] J. Xiao, S. Zou, Y. Yu, Y. Wang, T. Ding, Y. Zhu, J. Yu, S. Li, Z. Duan, Y. Wu et al., "3d recycled mortar printing: System development, process design, material properties and on-site printing," Journal of Building Engineering, vol. 32, p. 101779, 2020.

[11] F. Bos, R. Wolfs, Z. Ahmed, and T. Salet, "Additive manufacturing of concrete in construction: potentials and challenges of 3d concrete printing," Virtual and physical prototyping, vol. 11, no. 3, pp. 209–225, 2016.

[12] J. Reinold, V. N. Nerella, V. Mechtcherine, and G. Meschke, "Extrusion process simulation and layer shape prediction during 3d-concrete-printing using the particle finite element method," Automation in Construction, vol. 136, p. 104173, 2022.

[13] Z. Liu, M. Li, Y. Weng, Y. Qian, T. N. Wong, and M. J. Tan, "Modelling and parameter optimization for filament deformation in 3d cementitious material printing using support vector machine," Composites Part B: Engineering, vol. 193, p. 108018, 2020.

[14] M. P. Serdeczny, R. Comminal, D. B. Pedersen, and J. Spangenberg, "Experimental validation of a numerical model for the strand shape in material extrusion additive manufacturing," Additive Manufacturing, vol. 24, pp. 145–153, 2018.

[15] H. Zhang, J. Wang, Y. Liu, X. Zhang, and Z. Zhao, "Effect of processing parameters on the printing quality of 3d printed composite cement-based materials," Materials Letters, vol. 308, p. 131271, 2022.

[16] P. F. Yuan, Q. Zhan, H. Wu, H. S. Beh, and L. Zhang, "Real-time toolpath planning and extrusion control (rtpec) method for variable-width 3d concrete printing," Journal of Building Engineering, vol. 46, p. 103716, 2022.

[17] K. Wi, V. Suresh, K. Wang, B. Li, and H. Qin, "Quantifying quality of 3d printed clay objects using a 3d structured light scanning system," Additive Manufacturing, vol. 32, p. 100987, 2020.

[18] J. Villacrés, R. Guamán, O. Menéndez, and F. A. Cheein, "3d printing deformation estimation using artificial vision strategies for smart-construction," in IECON 2021–47th Annual Conference of the IEEE Industrial Electronics Society. IEEE, 2021, pp. 1–6.

[19] A. Kazemian, X. Yuan, O. Davtalab, and B. Khoshnevis, "Computer vision for real-time extrusion quality monitoring and control in robotic construction," Automation in Construction, vol. 101, pp. 92–98, 2019.

[20] O. Davtalab, A. Kazemian, X. Yuan, and B. Khoshnevis, "Automated inspection in robotic additive manufacturing using deep learning for layer deformation detection," Journal of Intelligent Manufacturing, pp. 1–14, 2020.

[21] A. Anton, L. Reiter, T. Wangler, V. Frangez, R. J. Flatt, and B. Dillenburger, "A 3d concrete printing prefabrication platform for bespoke columns," Automation in Construction, vol. 122, p. 103467, 2021.